

WS15-B02

4D Surface Wave Tomography Using Ambient Seismic Noise

F. Duret* (CGG) & E. Forgues (CGG)

SUMMARY

In 4D land seismic and especially for Permanent Reservoir Monitoring (PRM), changes of the near-surface induce unwanted signal variations that interfere with the 4D signal recorded from the reservoir. A three-month PRM pilot was carried out for Shell on the Peace River heavy oil field in Alberta, Canada in 2009. During this period, reservoir production was monitored using active buried sources and buried receivers. We took advantage of this continuous seismic recording to extract surface waves from recorded ambient noise using cross-correlation techniques. Surface wave tomography is then applied to produce daily time-lapse surface wave velocity maps that monitor velocity variations within the near-surface. We provide an image of the shallow subsurface velocities showing generally higher values in the southern part of the area. This pattern correlates fairly well with the known presence of swamp (muskeg) in the area and the wells pad location. Calendar observation of velocity maps shows stronger variation at low frequencies with good spatial coherence. In the case of PRM and continuous seismic monitoring, these findings could help to discriminate, at least qualitatively, contributions due to near-surface variations from actual reservoir 4D variations.

Introduction

In 4D land and especially for Permanent Reservoir Monitoring (PRM), changes of the near-surface induce unwanted signal variations that interfere with the 4D signal recorded from the reservoir. A three-month PRM pilot was carried out for Shell on the Peace River heavy oil field in Alberta, Canada in 2009. During this period, reservoir production was monitored using active buried sources and buried receivers. We took advantage of this continuous seismic recording to extract surface waves from recorded ambient noise using cross-correlation techniques. We show the ability of surface wave tomography to map the shallow subsurface velocity of the area. As a second step, the analysis is performed over the entire period of acquisition to produce time-lapse surface wave velocity maps that monitor velocity variations within the near-surface.

Acquisition spread and passive seismic data

The seismic dataset is an 84-day continuous recording of 734 vertical component geophones buried at 12 m below the free surface (see the white circles on Figure 1). This dataset was recorded during a continuous monitoring experiment conducted for Shell on a heavy oil field at Peace River, Canada (Forgues et al., 2011). Our patented multi-source emission allows us to simultaneously use active and passive seismic signals. This means that we not only build an image of the reservoir using “active” seismic (i.e., a seismic wavefield generated by dedicated sources), but we also record and extract background noise. This so-called noise is usually incoherent across the surveyed area, but can also contain a coherent seismic wavefield which we call “passive” seismic, as opposed to active seismic. This passive wavefield is generated by natural sources (ocean swell, rain, wind, etc.) or human activity (road traffic, industrial or reservoir activity), and can be transient (e.g., micro-earthquakes generated during reservoir evolution) or continuous (ocean swell, industrial activity, etc.).

In the present paper, we are interested in the continuous component of the passive wavefield, which is mainly composed of low frequency (< 10 Hz) surface waves (Ekström, 2001), and thus primarily contains information on the near-surface. This information is extracted by interferometry techniques (Bensen, et al., 2007) that consist of correlating receiver-to-receiver records to enhance common information in the pair of records (the signal that is actually propagated between the receivers) while discarding incoherent signals (e.g., electronic noise, local noise).

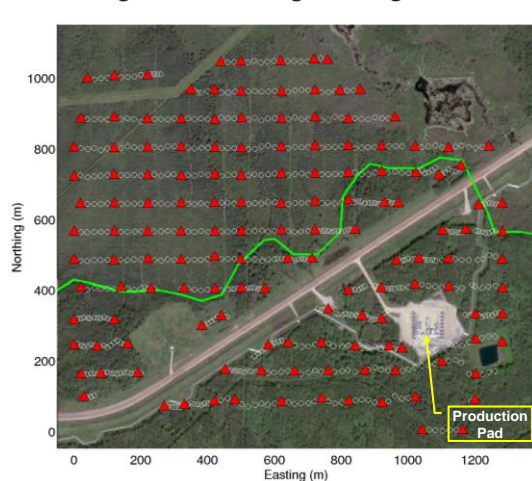


Figure 1: Satellite map of Pad-32 area, with selected receivers (red triangles) and assumed muskeg limit (green line).

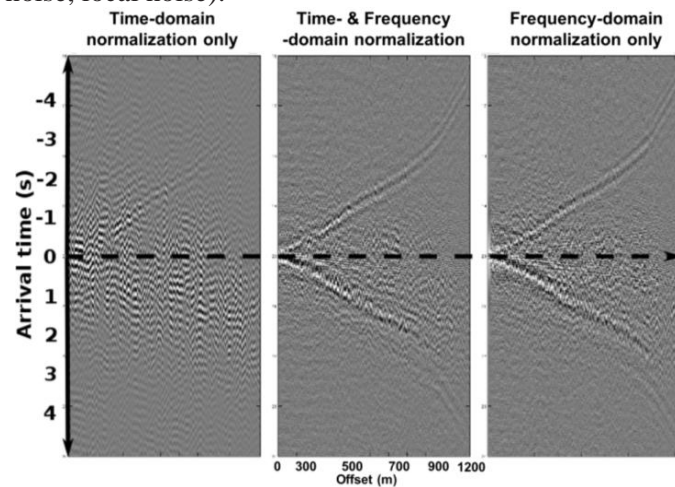
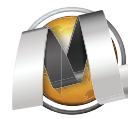


Figure 2: Results of pre-processing parameter testing for 3h of cross-correlations. Best result is obtained when only spectral-domain normalization is applied.

Surface waves present significant differences compared to body (P- and S-) waves. Firstly, they propagate along the surface of the medium whereas body waves propagate through the medium. Secondly, surface waves are dispersive, meaning that their propagation velocity will vary as a function of their frequency. At lower frequencies, surface waves usually have longer wavelengths and thus sample deeper layers and travel faster; whereas with shorter wavelengths, higher frequencies provide information on the shallowest parts of the medium and propagate with slower velocity. Thus the measurement of the propagation velocity of the surface waves between a pair of receivers at



different frequencies (e.g., the measurement of their dispersion curves) provides information on the vertical structure of the medium between that pair of receivers.

Passive wavefield reconstruction using seismic interferometry

As already mentioned, the passive wavefield is reconstructed by seismic interferometry: records are correlated from every possible pair of receivers composing our spread. In physical terms, we can interpret the operation as simulating a source located at the first receiver, whose signal has propagated through the medium and is recorded by the second receiver. In practice, the analysis of ambient noise interferometry in real-time requires the following steps:

1. The pre-processing of the raw data that includes:
 - Spatial down sampling with a selection of 144 receivers roughly spaced 80 m apart on a regular grid (red triangles on Figure 1)
 - Data filtering and down sampling to 10 ms to focus on low frequencies (< 10 Hz)
 - Frequency-domain normalization to remove strong transient events (see Figure 2, right)
2. The cross-correlation (CC) of every possible pair of the 144 selected receivers
3. The summation of the resulting CCs along a certain period of time (seven days) to enhance the SNR of the reconstructed wavefield to a usable signal. We obtained a total of 79 correlation panels covering the entire period of acquisition.
4. Reconstructed wavefield analysis, with a focus on reconstructed surface wave characterization.

Group velocity dispersion curve measurement

For every computed correlation pair, we sum the positive and negative lags and apply Frequency-Time Analysis (FTAN, Levshin et al. 1989) to measure the dispersion curve of reconstructed Rayleigh waves. FTAN consists in applying successive Gaussian filters on an analyzed trace to isolate wave train arrival times as a function of their frequency. The group velocity dispersion curve is measured by following the maximum of FTAN at each frequency. We finally apply instantaneous frequency correction to correct for local maximum misallocation induced by the application of Gaussian filters (Shapiro and Singh, 1999). This procedure is applied on all 10,296 pairs of correlations. Since the process is automated and can potentially result in a number of wrong measurements, we apply the following selections on measured dispersion curves:

- Velocities below 250 m/s or above 500 m/s are rejected.
- At least one wavelength and not more than 20 are within the inter-receiver distance.
- Dispersion curves lie within their median +/- standard deviation.

As a result, we obtained nearly 8,000 dispersion curves ranging from 1 to 8 Hz (Figure 3).

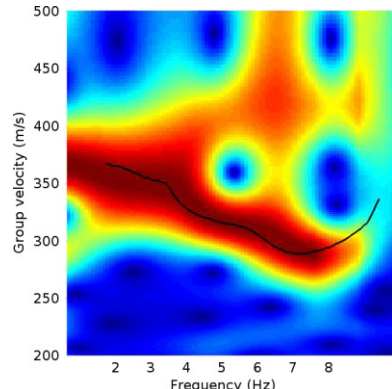


Figure 3: Time-Frequency Analysis and associated dispersion curve (black curve) for a 620 m offset receiver pair.

Continuous 4D surface wave tomography

For each frequency, discrete dispersion measurements are regionalized to infer surface wave velocity within the medium over a regular grid common to all frequencies. The tomography method we used is a least-squares method based on that proposed by Barmin et al (2001). It is based on ray theory with a Gaussian-shaped lateral smoothing. The method is fairly quick and robust but very dependent on the initial model, the inversion parameters and the lateral smoothing parameter. To mitigate these dependencies and to favor observation, we follow a data-driven approach:

- The initial constant velocity model is equal to the average velocity at the considered frequency.
- For all frequencies, lateral smoothing is estimated after the observed average wavelength: 60m.

In Figure 4, we present velocity maps obtained for five different dates from June to August at 4 Hz and 7 Hz respectively. We observe a general south-north trend, with a faster (~ 400 m/s) velocity

region in the southern part of the area, and a slower velocity (~ 350 m/s) in the north. This trend matches that observed by De Meersman (2011), who extracted the Q-factor from active seismic S-wave records. It also follows the known presence of muskeg (swamp) as indicated by the green line on Figure 1). The stronger velocity anomaly located in the south-east corresponds to the production well pad where a thick layer of gravel has been installed for the jack-pumps installations.

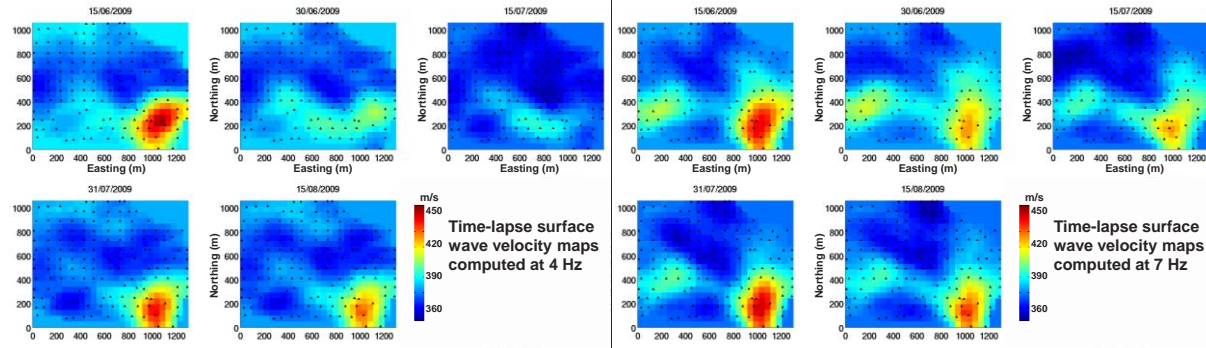


Figure 4: Time-lapse surface wave velocity maps computed at 4 Hz (left) and at 7 Hz (right). The southeast higher velocity pattern corresponds to the well pad location with a different soil (gravel).

Since the 4 Hz surface wave has a longer wavelength (~ 130 m) than the 7 Hz surface wave (~ 50 m), the 4 Hz map is sensitive to deeper features of the medium. Figure 5 displays calendar snapshots for each frequency along two lines. In Figure 6 we display, for each frequency, the daily measurement of velocity at three particular points. We observe the maximum velocity at 6 Hz and a similar calendar trend for the whole frequency range from 3 to 8 Hz: first a rapid velocity decrease from June 15th to June 30th then an increase followed by one month of stabilization. For the section located in the swamp area (Figure 6, “F”), only few calendar variations are noticeable.

In Figure 6, the “G” location corresponds to a bin located in the higher velocity anomaly of the well production pad. This is clearly where we observe the strongest velocity variation over the three month period. First the velocity decreases from June 15th to June 30th starting from the low frequencies up to 5 Hz. Then from end of June to 20th of July, little variation is observed. The inverse phenomenon is then observed from July 20th to July 31st with velocity gradually increasing, starting at higher frequencies and then ‘propagating’ towards low frequencies. This phenomenon is repeated once more in August. Therefore, although unusual, this observation of stronger variation at low frequencies than at high frequencies seems related to actual variations of the medium, which we do not explain, but could be related to the activity on the production pad. With longer calendar time periods, we could possibly observe longer term features such as icing de-icing cycles of the ground.

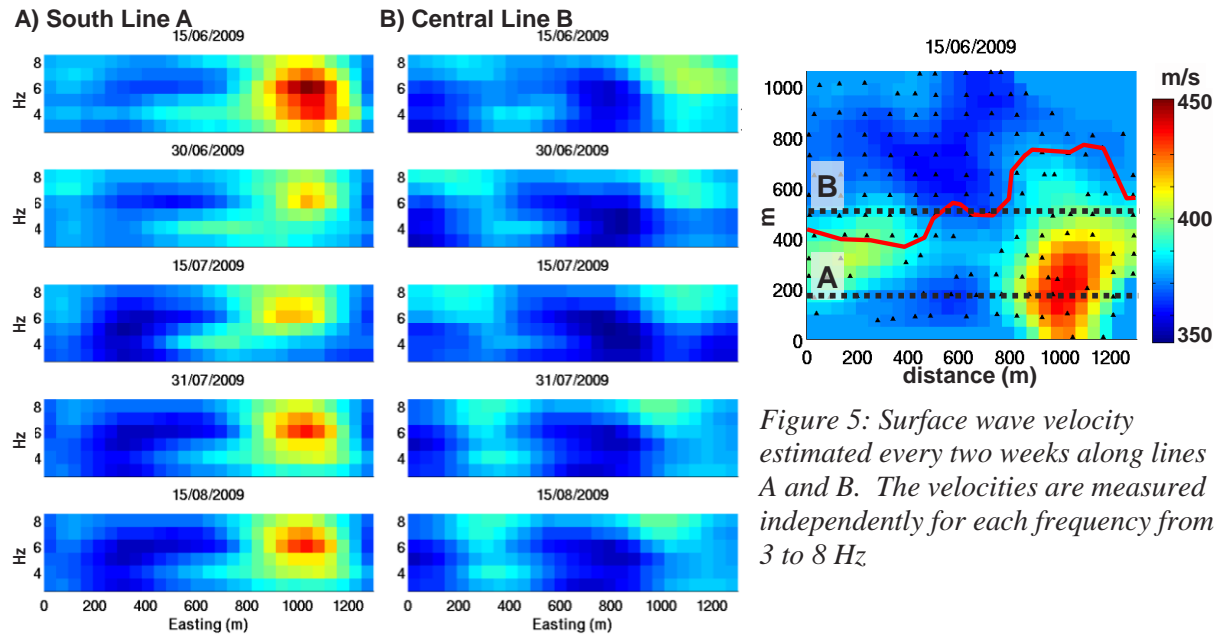


Figure 5: Surface wave velocity estimated every two weeks along lines A and B. The velocities are measured independently for each frequency from 3 to 8 Hz.

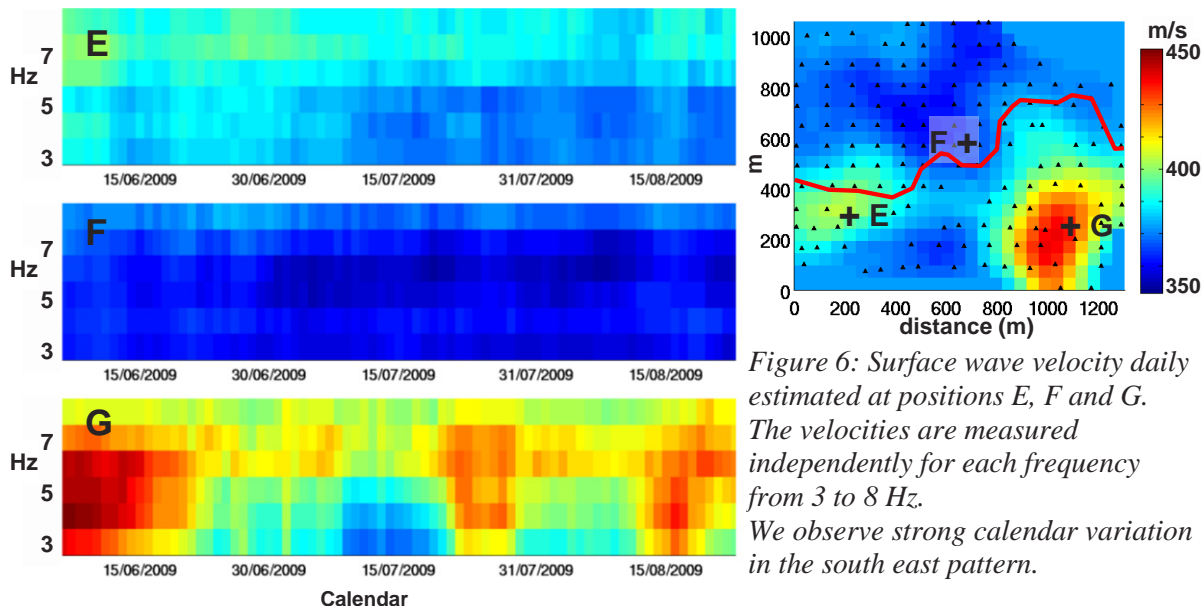


Figure 6: Surface wave velocity daily estimated at positions E, F and G. The velocities are measured independently for each frequency from 3 to 8 Hz. We observe strong calendar variation in the south east pattern.

Conclusion

Surface wave tomography using surface waves reconstructed by passive seismic interferometry has been applied on a continuous seismic acquisition dataset. The technique relies on the processing of noise data, and thus provides daily additional information which is independent from the active seismic. We provide an image of the shallow subsurface velocities showing generally higher values in the southern part of the area. This pattern correlates fairly well with the known presence of swamp (muskeg) in the area and the wells pad location. Calendar observation of velocity maps shows stronger variation at low frequencies with good spatial coherence. We are therefore confident in the ability of our technique to provide information of the near-surface (velocity variations with depth, space and calendar time). In the case of PRM and continuous seismic monitoring, these findings could help to discriminate, at least qualitatively, contributions due to near-surface variations from actual reservoir 4D variations.

Acknowledgements

We would like to thank Shell for their support and kind permission to present this work and Kees Hornman in particular for his very helpful input.

References

- Barmin, M., Ritzwoller, M. and Levshin, A. [2001] *A fast and reliable method of surface wave tomography*, Pure and Appl. Geophys., **158**: 1351-1375.
- Bensen, G., Ritzwoller, M., Barmin, M., Levshin, A., Lin, F., Moschetti, M., Shapiro, N., and Yang, Y. [2007] *Processing seismic ambient noise data to obtain reliable broad-band surface wave dispersion measurements*, Geophys. J. Int. **169**: 1239-1260.
- De Merrmann, K. [2011]. *High-resolution measurements of S-wave attenuation within the weathering layer of an Alberta heavy oil field*, EAGE 73rd Conference and Exhibition.
- Ekström, G. [2001]. *Time domain analysis of Earth's long-period background seismic radiation*, J. Geophys. Res., **106(26)**: 483-494;
- Forgues, E., Schisselé, E. and Cotton, J. [2011]. *Simultaneous active and passive seismic monitoring of steam-assisted heavy oil production*, TLE 1287-1294.
- Levshin, A., Barmin, M., Bukchin, B., Its, E., Lander, A., Ratnikova, L., and Yanovskaya, T. [1989]. *Seismic surface waves in a laterally inhomogeneous Earth*. Kluwer Academic Publishers.
- Shapiro, N. and Singh, S. [1999]. *A systematic error in estimating surface-wave velocity dispersion curves and a procedure for its correction*, Bull. Seismo. Soc. Am., **89**: 1138-1142.